JOURNAL OF GEOPHYSICAL RESEARCH, VOL. 103, NO. B5, PAGES 9931–9944, MAY 10, 1998

Hydrothermal fluid circulation through the sediment of Crater Lake, Oregon: Pore water and heat flow constraints

C. Geoffrey Wheat[1]
Institute of Marine Sciences, University of Alaska, Fairbanks

James McManus, Jack Dymond, and Robert Collier
College of Oceanic and Atmospheric Sciences, Oregon State University, Corvallis

Michael Whiticar
Centre for Earth and Ocean Research, University of Victoria, Victoria, British Columbia, Canada

Abstract. We present evidence for pore water flow through the sediment of Crater Lake, Oregon based on systematic variations in pore water chemical compositions and thermal gradients. Pore water was extracted from sediment by centrifugation and diffusive exchange using a gravity corer deployed from a surface vessel and a box corer and peepers deployed from the submersible *Deep Rover* in a known geologic context. Depth profiles of sediment temperature were measured using two probes deployed from the submersible. One probe was connected to the submersible whereas the other was self-contained and deployed for 7 days. On the basis of measured and calculated depth profiles of pore water Na, Ca, Mg, K, Li, and temperature, we show that pore water upwells in zones of focused upflow at speeds of meters to hundreds of meters per year. These zones of focused flow are patchy and usually cover several square meters to hundreds of square meters and are marked by iron-manganese-rich crusts, bacterial mats, and saline pools. In contrast, most of the lake floor consists of sediment derived from the caldera walls and has a low heat flow with pore water velocities of millimeters per year. The chemical composition of the pore water that upwells through the sampled section of the sediment column differs from core to core. This difference results from mixing a hydrothermal fluid in igneous basement below the lake with lake water before the final ascent through the sediment column. Elemental ratios of this thermally and chemically altered fluid in basement match those calculated based on mass balance considerations. Calculation of mass balance and geothermometry constrain the temperature in basement and ultimately the power output, which is about 30 MW. This power output is in agreement with two other estimates that were calculated using temperature data from the water column and measurements of sediment heat flow.

1. Introduction

Crater Lake, Oregon is located in the southern section of the Cascade mountain range (Figure 1) in the completely enclosed caldera of Mount Mazama, an andesitic volcano. Crater Lake formed shortly after a cataclysmic eruption roughly 6850 years B.P. [*Bacon*, 1983] and volcanic activity continued for several thousand years with the last eruption about 4000 years B.P. [*Bacon and Lanphere*, 1990]. These eruptions formed Wizard Island, Wizard Platform, and Merriam Cone (Figure 1). This volcanism was accompanied by hydrothermal activity as indicated by the alteration of andesitic stockwork [*Barber and Nelson*, 1990]. Recent evidence supports the hypothesis that chemically and thermally altered water relative to lake water is presently issuing into the lake. Evidence includes anomalously high concentrations of Cl and sulfate in Crater Lake relative to concentrations in neighboring lakes [*Van Denburgh*, 1968], chemical and physical data from the water column [*Simpson*, 1970a,b; *Dymond et al.*, 1989; *Dymond and Collier*, 1990; *Collier et al.*, 1990a,b; *McManus et al.*, 1992, 1993, 1996], measurements of heat flow [*Williams and Von Herzen*, 1983], and calculations of mass balances [*Nathenson*, 1990].

All of the above work provide indirect evidence for input of chemically and thermally altered water into Crater Lake. In 1989, submersible operations were employed to find sites of active venting of hydrothermal fluids, such as water issuing from chimney-like features, mud volcanos, shimmering water, or non linear profiles of sediment temperature. In this paper we present direct evidence for hydrothermal pore water flow through the sediment of Crater Lake based on systematic variations in pore water chemical compositions and thermal

[1]Now at West Coast and Polar Regions Undersea Research Center, Moss Landing, California.

Paper number 97JB03391.
0148-0227/98/97JB03391$09.00

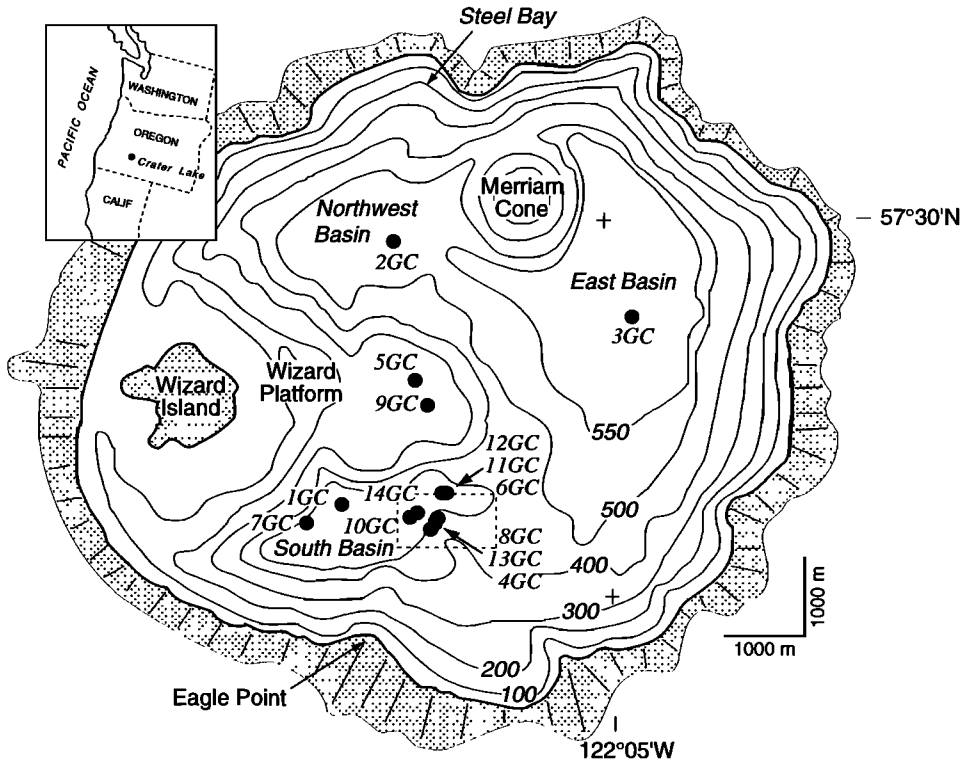

Figure 1. Location of gravity cores (GC) in Crater Lake, Oregon. Bathymetric contours are 100 m. The box defines the area represented in Figure 2.

gradients. These pore water data provide a measure of the speed of pore water flow through the sediment, constrain the pattern of fluid circulation through the sediment and underlying basement, and allow us to estimate the composition of the fluid in basement and the flux of dissolved chemical species, heat, and water from basement to the deep lake.

2. Benthic Setting

Crater Lake, Oregon, is enclosed by caldera walls, which rise hundreds of meters above the caldera floor and are composed of basaltic andesite [*Bacon and Lanphere*, 1990]. These walls define the drainage basin, obstruct surface outflow, and restrict sedimentary inputs. Sediment in Crater Lake is mostly aluminosilicate debris. Net accumulations of aluminosilicate debris, biogenic debris from the euphotic zone, and iron-manganese-rich precipitates from input of hydrothermal water at the lake bottom [*Dymond and Collier*, 1990] differ from tens of centimeters on the slopes of the caldera walls to several meters on Wizard Platform to about 100 m in basement depressions [*Barber and Nelson*, 1990].

Most of the lake floor is covered by a smooth layer of aluminosilicate debris that is undisturbed by benthic organisms. In the South Basin, other sedimentary and biological features were observed. For example, we located and sampled iron-manganese-rich crusts that contain about 35 weight per cent (wt %) Fe and less than 1 wt % Al. These crusts form multi colored pavements (ochre to dark brown) that cover tens to hundreds of square meters, fields of pebbles that also cover tens to hundreds of square meters, and multiple ochre-colored layers that are visible in areas of sediment slumping [*Dymond and Collier*, 1990]. Other features that were sampled include bacterial mats, which are 2 to 20 m in length and several meters across and are mostly composed of iron-oxidizing, sheath-forming bacteria of the genera *Gallionella* and *Leptothrix* [*Dymond et al.*, 1989] and saline pools, which have salinities and temperatures that are greater than that measured in the surrounding lake water. A more detailed physical, chemical, and thermal description of the mats and pools is given by *Collier et al.* [1991].

3. Methods

Sediment and pore water was sampled using a gravity corer, a box corer, "peepers," and two temperature probes to characterize profiles of the chemical composition and thermal gradient of pore water and to quantify sediment physical properties. Gravity cores (GC) up to 170 cm in length were collected from a surface vessel. These cores were used to target general areas of interest where longer sediment sections were desired. Box cores (BC), "peepers" (letters A through H, Figure 2), and temperature probes were used to target specific sedimentary features in a known geologic setting using the submersible *Deep Rover*. Niskin bottles also were deployed from the submersible to collect water from mats and pools on the lake floor and are reported as lake floor spring samples herein.

Sediment samples for pore water extraction were taken from 14 gravity cores (Figure 1) and 8 box cores, which were 0.06 to 0.2 m in length (Figure 2). Gravity cores were packed in snow and transported to a van, held at 3° -5°C where they were split, described, and sampled for sediment physical properties and for pore water extraction by centrifugation within 12 hours of retrieval. Box cores were retrieved using a miniature Soutar-type box corer that was developed for deployment by a submersible [*Soutar et al.*, 1981]. These cores were packed in snow and sampled immediately by whole-core squeezing

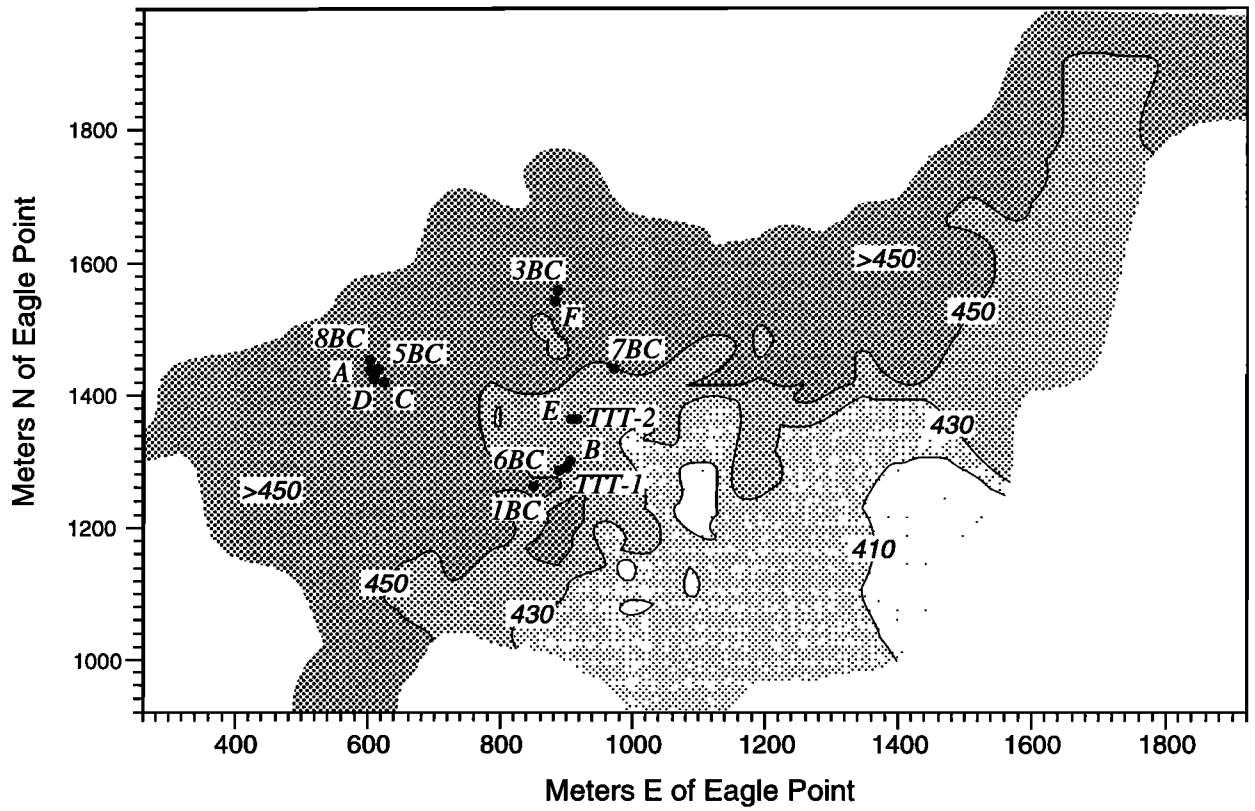

Figure 2. Location of box cores (BC), peepers (Letters A through F), and TTT deployments with respect to bathymetry (20 m contours). The location of Eagle Point is shown in Figure 1. Two of the eight box cores were collected out of this area.

[*Bender et al.*, 1987]. In addition, discrete sediment samples were taken near the base of these cores and stored in snow for 3-15 hours until they could be centrifuged.

Supernatant from centrifuged sediment and pore water extracted by whole-core squeezing were filtered through 0.45 μm filters and subsampled into several aliquots. Aliquots for Cl and sulfate were sealed in glass ampules. Aliquots for Na, Ca, Mg, K, and Li (4-6 mL) were spiked with 10 μL of redistilled 1 *N* hydrochloric acid and stored in acid-washed, high-density polyethylene bottles. An additional aliquot was stored in polystyrene test tubes for analysis of nutrients, *p*H, and total CO_2, all of which were measured within 1 to 2 days of core retrieval. Some of these data are omitted in this paper because they do not provide additional arguments for the principal hypothesis of hydrothermal circulation in Crater Lake, Oregon.

Pore water was collected with "peepers" to obtain samples that were not chemically altered by sampling procedures. Peepers were made from 1.27 cm thick polycarbonate sheets in which cavities 1 cm in length were milled every 2 cm down the length of the sampler. These cavities hold about 4.5 mL of water, and two cavities were milled at each sample depth. Cavities were filled with deoxygenated distilled water and covered by a 0.45 μm dialysis membrane. Peepers were stored in deoxygenated distilled water until they were inserted into the sediment. A plastic T handle was attached to the peeper to aid in deployment, and the bottom edge of the peeper was beveled to cause minimal sediment disturbance. Four peepers with 20 cavities and one peeper with 36 cavities were deployed for about 1 week (Figure 2), during which time water in the cavities equilibrated with adjacent pore water via diffusion. Aliquots of pore water from the peepers were taken upon retrieval and stored in vacutainers. One aliquot was spiked with 10 μL of redistilled 1*N* hydrochloric acid and analyzed for several metals. Si was measured on a different aliquot.

Dissolved silica was measured using a standard colorimetric technique [*Parsons et al.*, 1984] with a precision of about 2% (1σ). Concentrations of Cl were determined by ion chromatography with a precision of <2% (1σ). Atomic absorption spectrometry techniques were used to measure concentrations of Na, Ca, Mg, K, and Li with precisions of less than 5% and typically less than 2% (1σ). Some sampling and/or storage artifacts exist. For example, the concentration of Na increased by 0.3 m*M* in all of the peeper samples, which were stored in glass vacutainers. This result is based on a systematic offset observed in plots of Na versus Li for peeper samples versus box core, lake floor spring, and gravity samples, which were stored in plastic. Similarly, concentrations of K are 0.02 m*M* higher in pore water processed by centrifugation relative to those from peepers and lake floor springs as indicated by a positive offset of 0.02 m*M* K in the upper-most samples from gravity cores. This artifact probably results from ion-exchange reactions that occur as a result of changes in temperature and pressure during sample handling [*de Lange et al.*, 1992].

Two temperature probes were used, one of which is 60 cm in length with thermistors mounted at 20, 40, and 60 cm along the probe. The resolution of each thermistor is 0.01°C with an accuracy of ± 0.2°C, and the thermistors were calibrated against known resistance values periodically throughout the sampling program. This probe was connected to an Omega Model 5830 Thermistor Thermometer in the submersible. Temperature measurements were recorded on the video record of the operation. This record was then used to determine the depth of

penetration. Forty-eight temperature measurements were made; however, 28 of these measurements were made with only one thermistor inserted into a particular feature. Impenetrable crusts or underlying rocks are the likely causes of incomplete penetration of the probe.

We also used a Sea-Bird Electronics SeaCat SBE 19 Temperature Profiler (TTT) with three thermistors epoxy-potted inside a 61 cm long, 0.635 cm diameter stainless steel tube. When fully inserted into the sediment, thermistor depths are 35 and are 5 cm below the sediment-water interface and 5 cm above the sediment-water interface. The SeaCat profiler recorded temperature profiles 2 times a second with a resolution of 0.001°C and an accuracy of ±0.01°C over a temperature range of -5°C to 35°C. All three thermistors registered identical temperatures during descent. Only after the initial penetration did the temperature readings diverge in response to thermal gradients within the sediment. All three thermistors registered identical temperatures during transit to the second site and during ascent. The TTT recorded data continuously at one site (TTT-1) for 3 days and at a second site (TTT-2) for 4 days (Figure 2).

4. Models for Pore Water Data

Pore water depth profiles of Na from representative cores are shown in Figure 3. Profile shapes of Ca, Cl, Mg, Li, K, and Si concentrations in pore water from box cores and peepers parallel the shape defined by Na data. Likewise, chemical profile shapes of pore water data from gravity cores generally parallel Na profiles. The clear exception is Si (Figure 3). For example, the profile of Si from GC 1 is curved, but the Na profile is linear, suggesting that different processes control the shape of these profiles. Chemical and thermal profiles of pore water are influenced by time-dependent, diffusive, advective, and reactive processes. For the one-dimensional case a mathematical representation of these processes is

$$\partial(\phi C)/\partial t = \partial(\phi D_s(\partial C/\partial z))/\partial z - \partial(\phi v C)/\partial z + \phi \Sigma R, \quad (1)$$

time = diffusion + advection + reaction

where ϕ is porosity, C is concentration, t is time, D_s is the sediment diffusion coefficient, z is depth (positive down core),

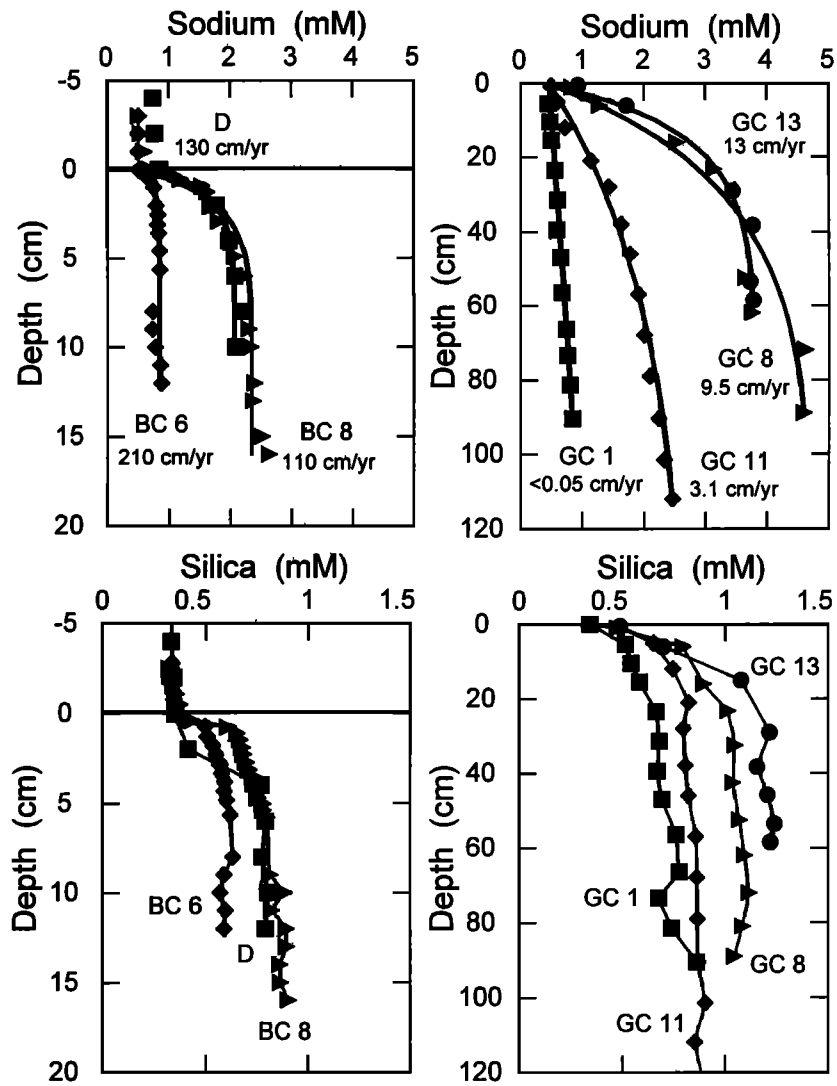

Figure 3. Profiles of pore water Na and Si from representative cores. Curves shown in plots with the Na data were calculated from equation (5), and speeds of pore water upwelling are identified. Lines connect the Si data. Note the difference in the depth scales.

v is velocity (upwelling is negative), and ΣR includes all terms related to biogeochemical interactions influencing a particular solute or temperature [*Berner*, 1980]. This model is simplified by evaluating the relative importance of each term and eliminating insignificant terms. In the following discussion we present arguments that support an advection-diffusion model for chemical species that are "conservative" in the sediment column and for temperature and an advection-diffusion-reaction model for Si, which is non conservative in the sediment section collected with gravity cores.

4.1. Chemical Profiles

The diffusive term is a function of the sediment diffusion coefficient, which varies with temperature, tortuosity, and electrical effects [*Berner*, 1980]. For calculating the diffusive term, we used the temperature of bottom lake water, even though the maximum temperature recorded in hydrothermal features is about 4° to 15°C above ambient (Table 1). Our rational for using lake water temperature is that no measurements of temperature were made where gravity cores were taken and the maximum temperature where box cores were retrieved from specific geologic features was less than 10°C. This difference in temperature results in an increase in the sediment diffusion coefficient by at most 40% [*Li and Gregory*, 1974]. Because gravity cores were not collected from geologic features, the temperature would be less and thus have less of an effect on the diffusion coefficient. In contrast to the temperature effect the down core change in tortuosity, which is a function of the formation factor and porosity and is numerically estimated by Archie's law [*McDuff and Ellis*, 1979], results in a decrease in the sediment diffusion coefficient. This decrease, which is about 24%, stems from a decrease in porosity from about 0.85 near the sediment-water interface to about 0.65 at 1.7 m below the lake floor. Electrical effects, which cause the more mobile ions to diffuse slower and the less mobile ions to diffuse faster [*Berner*, 1980], are produced by gradients of charged ions generating an electrical potential while maintaining electroneutrality. This effect was not included in the calculations, because the lack of a calculated charge balance resulting from incomplete analyses and errors in using pH and total CO_2 data to estimate alkalinity in some samples makes these corrections equivocal. Because of the uncertainties in estimating changes in temperature and porosity and calculating charge balance, we used a uniform sediment diffusion coefficient with depth based on the coefficients listed by *Li and Gregory* [1974] adjusted to the temperature of deep lake water (3.7°C) and accounting for Archie's Law with a uniform porosity of 0.85. Using a uniform diffusion coefficient does not alter the general results or conclusions based on the model calculations.

We simplified (1) further by examining the need for a time-dependent term. For example, if we assume that the concentration of lake water changed from 4 mM Na to its present value of about 0.5 mM for a range of times before present, then calculated profiles based on diffusive and time-dependant terms can approximate measured profiles (Figure 4). However, a range of timescales is required, inconsistent with a well-mixed lake with a stable chemical composition for the past 50-100 years [*Nathenson*, 1990]. We also have calculated profiles in which the concentration of Na in the basement fluid has changed. These calculated profiles do not match measured profiles (Figure 4b). Thus time-dependant processes have been excluded from the models.

Table 1. Temperature Profiles Obtained From Specific Geologic Features Using the Temperature Probe

Dive	Sample Type	X, m	Y, m	T_1, °C	Z_1, cm	T_2, °C	Z_2, cm	T_3, °C	Z_3, cm	Velocity, cm yr^{-1}
	bottom water			3.74						
CD 216	sediment	609	1431			4.46	40	4.54	60	-3000
CD 217	sediment	978	1664	3.78	20	3.96	40	4.08	60	
CD 218	sediment	1040	1253	4.16	10			5.86	50	
CD 222A	sediment	924	1337	5.55	30	6.35	50	6.92	70	-1000
CD 222B	sediment	949	1438	4.21	20	4.72	40	5.33	60	
CD 222C	sediment	945	1361	5.00	25	5.85	45	6.65	65	-400
CD 223	sediment	539	1207	3.80	15	4.05	35	4.24	55	
CD 226	sediment	1062	1363	5.30	20	7.90	40	10.20	60	
CD 228A	sediment	2884	6062	4.60	2.0	10.20	22	10.80	42	-6000
CD 228B	sediment	2917	5954	3.68	-5.0	6.10	15	8.85	35	-500
CD 228C	sediment			3.68	-10	5.80	10	9.77	30	-200
CD 228D	sediment			3.69	-5.0	6.37	15	9.66	35	-300
CD 207	mat	843	1528	7.56	30	7.76	50	8.10	70	-3000
CD 215	mat	951	1150			9.00	10	9.60	30	-14000
CD 226	mat	999	1327	7.50	12	11.08	32	12.90	52	-2200
CD 228	mat	2884	6062	5.60	15	7.15	35	8.11	55	-1600
CD 230	mat	612	1421	4.84	10	5.75	30	6.00	50	-4000
CD 211	pool	634	1452			4.35	20	4.45	40	-6000
CD 228	pool	2907	5984	4.60	20	5.00	40	5.60	60	-500
CD 230	pool	618	1420	4.30	10	5.00	30	5.21	50	-3000

Fluid velocities are estimated by fitting the data to manipulations of equation (9). Upwelling is negative. Negative depths are distances above the sediment-water interface. X is the distance north of Eagle Point, and Y is the distance east of Eagle point. No entry denotes either no navigation or inconclusive results, which could in part be a result of a pore water velocity that is less than several hundred centimeters per year.

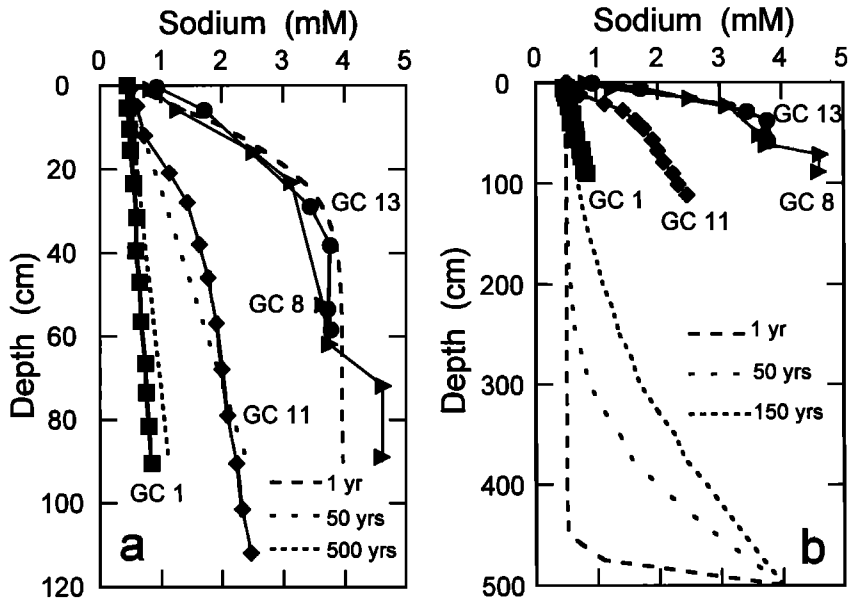

Figure 4. Representative profiles of Na plotted with profiles calculated with a time dependent-diffusion model. Calculated profiles at several time increments are shown that represent (a) a change in a uniform pore water profile of 4 m*M* Na to the present-day concentration of 0.5 m*M* Na in bottom lake water and (b) a change in a uniform pore water profile of 0.5 m*M* Na to a concentration of 4 m*M* Na at a depth of 5 m. Although measured data fit calculated profiles in Figure 4a, no changes in the Na concentration of the lake waters have been observed in recent years [*Nathenson*, 1990]. Changes in the composition of the basement fluid generate concave up profiles in contrast to the many observed profiles with concave down shapes. Therefore time-dependant processes have been eliminated from models of pore water in Crater Lake, Oregon.

Is there a need for a reaction term? Terms for reaction are typically included for profiles of dissolved chemical species that are influenced by sediment-water reactions. For example, dissolution of amorphous silica in sediment increases the concentration of Si above values in deep lake water. Once steady state is reached, the concentration of Si remains uniform with depth [e.g., *Boudreau*, 1990; *Wheat and McDuff*, 1994]. Similar profiles of Si as well as other dissolved ions (e.g., Na, Cl, Mg, Ca, Li, and K) were observed in Crater Lake (Figure 3). If we assume that these profiles are governed by only diffusive and reactive processes with a reaction term that is first order with respect to the degree of undersaturation ($k(C-C_{ss})$, where k is the first-order rate constant and C_{ss} is the steady state concentration), then calculated rates of reaction for Na, Cl, Mg, Ca, Li, and K range from about 10^{-14} s^{-1} in GC 1, to 10^{-9} s^{-1} in GC 11, to 10^{-8} s^{-1} in GC 8 and GC 13, to 10^{-6} s^{-1} in box core and peeper samples. Rates of reaction vary with temperature and mineral assemblages. Yet, this calculated range is not consistent with a temperature change of at most 15°C and a single sedimentary source (primarily weathered andesite from the caldera walls). Furthermore, calculated chemical fluxes from the sediment using this model are orders of magnitude greater than measured values of burial fluxes (Table 2). Thus models of ion profiles must include an advective term.

Although sediment-water reaction may exist in some cores for some ions (i.e., Si in gravity cores), no reaction term is included in the following analysis. This does not preclude low-temperature water-rock reactions below the sampled section or reactions in the sediment section. The analysis presented above confirms that the resulting flux generated by any sediment-water reactions, which must be relatively uniform over the area sampled, is negligible for some elements (e.g., Cl, Na, and Li) relative to advective fluxes in some cores.

In the text that follows, we will use the pore water chemical data to calculate upwelling speeds. We will show that the cores listed in Table 2 have upwelling pore water speeds that range from several to hundreds of centimeters per year. As suggested by Table 2, the advective flux is orders of magnitude greater than a flux that could be generated from reaction. Thus we conclude that the pore water with the fastest upwelling speed is the least altered relative to the original composition of the fluid that entered the sediment section and that this original pore water at the base of the sediment section exhibits "conservative" mixing with lake water. Therefore, by eliminating the reaction term and avoiding elements that are highly reactive (e.g., Si), we can use the pore water data to calculate pore water upwelling speeds and to constrain the composition of the fluid below the

Table 2. Pore Water Chemical Fluxes From the Sediment to the Overlying Water Column Based on a Reaction-Diffusion Model and Compared with Burial Rates

Chemical Species	BC 8	PD	BC 6	GC 13	Burial Rate[a]
Na^+	200	83	25	18	1.4
Ca^{2+}	50	19	5.7	2.7	0.87
Mg^{2+}	8.2	29	5.3	2.5	0.82
K^+	19	8.2	4.9	2.8	0.38
Li^+	2.3	9.1	0.46	0.29	0.0058
Si	32	17	8.5	4.6	1.4

Values are given in $\mu M\ cm^{-2}\ yr^{-1}$.
[a]*Dymond and Collier* [1990].

Table 3. Vertical Fluid Velocities Estimated From the Pore Water Data and Manipulations of Equation (5)

Core	Chemical Species						Best Estimate
	Na^+	Ca^{2+}	Mg^{2+}	Cl^-	K^+	Li^+	
GC 1	±0.05	-0.6	±0.05	±0.05	±0.05	±0.05	±0.05
GC 8	-9.5	-5.2	-4.0	-11	-16	-10	-9.0
GC 11	-3.1	-1.5	-1.4	-3.6	-3.6	-1.5	-3.0
GC 13	-13	-9.6	-8.0		-12	-7.0	-11
PD	-130	-100	-80		-200	-110	-120
BC 6	-210			-220	-220	-240	-220
BC 8	-110			-150	-120	-80	-120

Upwelling is negative. No entry for Cl^- denotes insufficient data. Because of sampling artifacts, no velocities were calculated for Ca^{2+} and Mg^{2+} from box cores. Velocities are given in cm yr^{-1}.

sediment section. Eliminating the term for reaction reduces (1) to

$$D_s(\partial^2 C/\partial z^2) - v(\partial C/\partial z) = 0. \quad (2)$$

The solution to (2) given the following boundary conditions:

$$C = C_o \qquad z = 0, \quad (3)$$

$$C = C_{bot} \qquad z = z_{bot}, \quad (4)$$

is

$$C = C_o - A_1 + A_1 \exp(vz/D_s), \quad (5)$$

where

$$A_1 = \{C_{bot} - C_o\}/\{\exp(vz_{bot}/D_s) - 1\},$$

C_{bot} is the concentration at the base of the core and z_{bot} is the length of the sampled section.

Velocities of pore water flow through the sediment are calculated by minimizing the deviation between measured profiles and those calculated using (5) and a range of velocities (Figure 3 and Table 3). A measure of the uncertainty in these velocities is estimated by the value of the reduced χ^2, which is the sum of the deviations squared divided by the variance. The best fit to the data results when the reduced χ^2 is less than the 5% value, which means that the parameters used in calculating a profile have a high probability of being the correct set of parameters that describes the observed profile. Two examples are shown in Figure 5 for a range of upwelling speeds and sediment diffusion coefficients. These examples illustrate the uncertainties in modeling chemical profiles from areas with pore water upwelling speeds of the order of centimeters per year compared with larger uncertainties when estimating velocities of hundreds of centimeters per year. Note that at the slower velocities the estimated velocity is well constrained. For faster upwelling speeds the larger uncertainty results from having fewer data in the curved portion of the profile. In addition, uncertainties are greater for higher upwelling speeds because diffusion after core retrieval and disturbance of the sediment-water interface will alter the upper several millimeters of the profile [*Wheat and McDuff*, 1995]. Diffusion and disturbance tend to decrease the in situ gradient resulting in calculated velocities that are minima. In areas where pore water upwells at speeds greater than several hundred centimeters per year, better estimates of velocity are obtained using profiles of temperature.

Table 3 presents pore water velocities that were calculated using data from six different chemical species. Differences in calculated velocities result from uncertainties in the calculated diffusion coefficient, the quality of analytical measurements, the number of measurements from the curved portion of the profile, the presence of sediment-water reactions in the sampled section, and artifacts induced by sampling techniques. For example, dissolution of carbonates in GC 1 causes the calculated

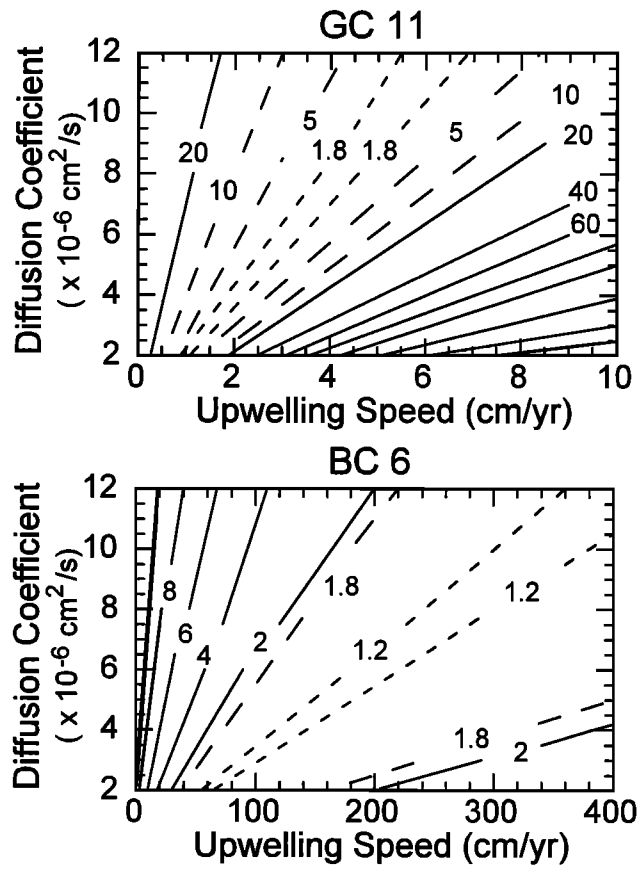

Figure 5. Contour plots of reduced χ^2 as a function of the sediment diffusion coefficient and upwelling speed for Na data from two representative cores: GC 11 and BC 6. The 5% reduced χ^2 value is 1.8 using a variance of 0.0021 mM^2 that is calculated from concentrations of pore water in uniform sections of profiles. Values greater than 1.8 represent a low probability for the given parameters to be the correct parameters for the model. These plots illustrate the larger uncertainty in estimating upwelling speed at speeds greater than several hundred centimeters per year, primarily because of continued diffusion after core retrieval [*Wheat and McDuff*, 1995] and the lack of data in the curved portion of the profile.

upwelling speed based on the Ca profile to be an order of magnitude greater than the speed estimated from the other ions. Similarly, whole-core squeezing causes an increase in the concentration of Ca and Mg relative to Na because of dissolution or adsorption-exchange reactions that occur as pore water is forced through the overlying sediment [*Bender et al.*, 1987]. Further, the analytical uncertainty is smaller for Na than for Cl or Li, and we have greater down-core coverage for Na than for these other elements. Because of the varied quality and quantity of data from which these velocities are calculated, an average of the calculated velocities is not appropriate, and the best estimate that is reported in Table 3 is heavily weighted to the Na result.

4.2. Temperature Profiles

Data from 28 temperature profiles are presented in Table 1. These data are compared to profiles calculated from the following advection-diffusion equation in one dimension:

$$D_T(\partial^2 T/\partial z^2) - v(\partial T/\partial z) = 0, \quad (6)$$

where T is temperature (in degrees Celsius) and D_T is the thermal diffusivity (2×10^{-3} cm^2 s^{-1} [*Williams and Von Herzen*, 1983]). Given the following boundary conditions:

$$T = T_0 \qquad z = 0, \quad (7)$$

$$T = T_{bot} \qquad z = z_{bot}, \quad (8)$$

the solution to (6) is

$$[T\text{-}T_0]/[T_{bot} - T_0] = [1 - \exp(vz/D_T)]/[1 - \exp(vz_{bot}/D_T)]. \quad (9)$$

Pore water velocities are estimated by minimizing the squared deviation of the data to calculations of (9) that employ a variety of velocities and a T_0 of 3.74°C (Figure 6 and Table 1).

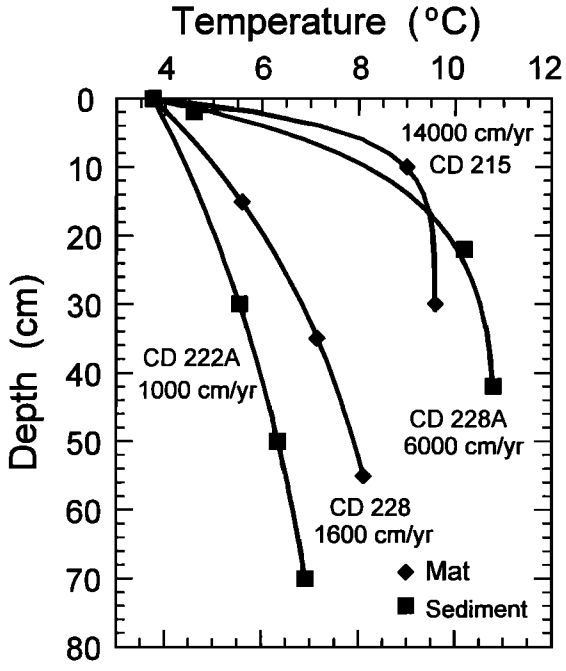

Figure 6. Representative profiles of temperature plotted with calculated profiles using equation (9). Upwelling pore water speeds are listed.

T_0 differs by at most 0.3°C in the deep lake, based on conductivity-temperature-pressure measurements from the submersible [*McManus et al.*, 1993] and by recordings of the TTT thermistor probe that rests 5 cm above the sediment-water interface (Figure 7). Calculated velocities range from less than several hundred centimeters per year to greater than 10,000 cm yr^{-1}. Uncertainties in the depth and angle of penetration and the possibility of having lake water seep into the sediment during insertion of the probe affect the precision of calculated velocities. For example, if the depth of penetration of CD 222 or CD 230 (Table 1) is ±3 cm or the angle of penetration is 30°, then the calculated velocity is ± 25% of the value listed in Table 1. Errors in the depth and angle of penetration are less than those listed above.

Twenty-eight other attempts to obtain temperature profiles resulted in having only one thermistor penetrate the sediment. Eighteen measurements were made in bacterial mats where the highest temperature recorded was 18.9°C, and six of the 18 measurements were greater than 10°C at a depth of less than 20 cm. Nine measurements were made in iron-manganese-rich sediment where temperatures range from 10.5° to 11.2°C. The remaining measurement was made in a pool at 6.45°C. No pore water velocities were calculated from these data, but they probably are faster than speeds reported in Table 1.

The TTT temperature probe was deployed for 1 week (Figure 7). Measured temperatures were uniform for the first 2 days of deployment, but on the third day, higher temperatures were recorded by the two thermistors near the sediment-water interface, reflecting either a change in the upwelling speed or a change in the depth of penetration produced by the probe settling into the sediment. After 3 days the TTT probe was moved 30 m away to an area where higher temperatures were recorded in the water column and in the sediment where it remained for 4 days. During these 4 days the three thermistors recorded temperatures that were about 0.8°C warmer than those recorded during the first 3 days of deployment. These warmer measurements for the uppermost probe, which is normally 5 cm above the sediment-water interface, are greater than the measured range of deep lake water temperature (3.5° to 3.9°C). This is not an instrument offset, because all of the thermistors measure 3.56°C when they were exposed to deep lake water both before and after deployment. Instead, this difference is a product of the probe penetrating deeper into the sediment than was planned. The depth of penetration was adjusted based on visual observations and a bottom water temperature of 3.9°C [*McManus et al.*, 1993] in calculations using (9) for minimizing the least squared deviation to the data (Table 4).

5. Pattern of Fluid Circulation

5.1. Pore Water Flow Through the Sediment-Water Interface

The spatial distribution of pore water flow from the sediment to the deep water of Crater Lake is characterized by two distinct settings. One setting covers much of the lake bottom where measurements of heat flow are relatively low (about 0.14 W m^{-2} [*Williams and Von Herzen*, 1983]) and sediment pore water velocities are tenths of a centimeter per year. In contrast, the other setting consists of sites several square meters to several hundreds of square meters with iron-manganese-rich crusts and bacterial mats, high heat flows of tens of watts per square meter, and pore water velocities that range from tens of centimeters per year to greater than tens of thousands of centimeters per year. Further, pore water flow from these sites differs markedly over

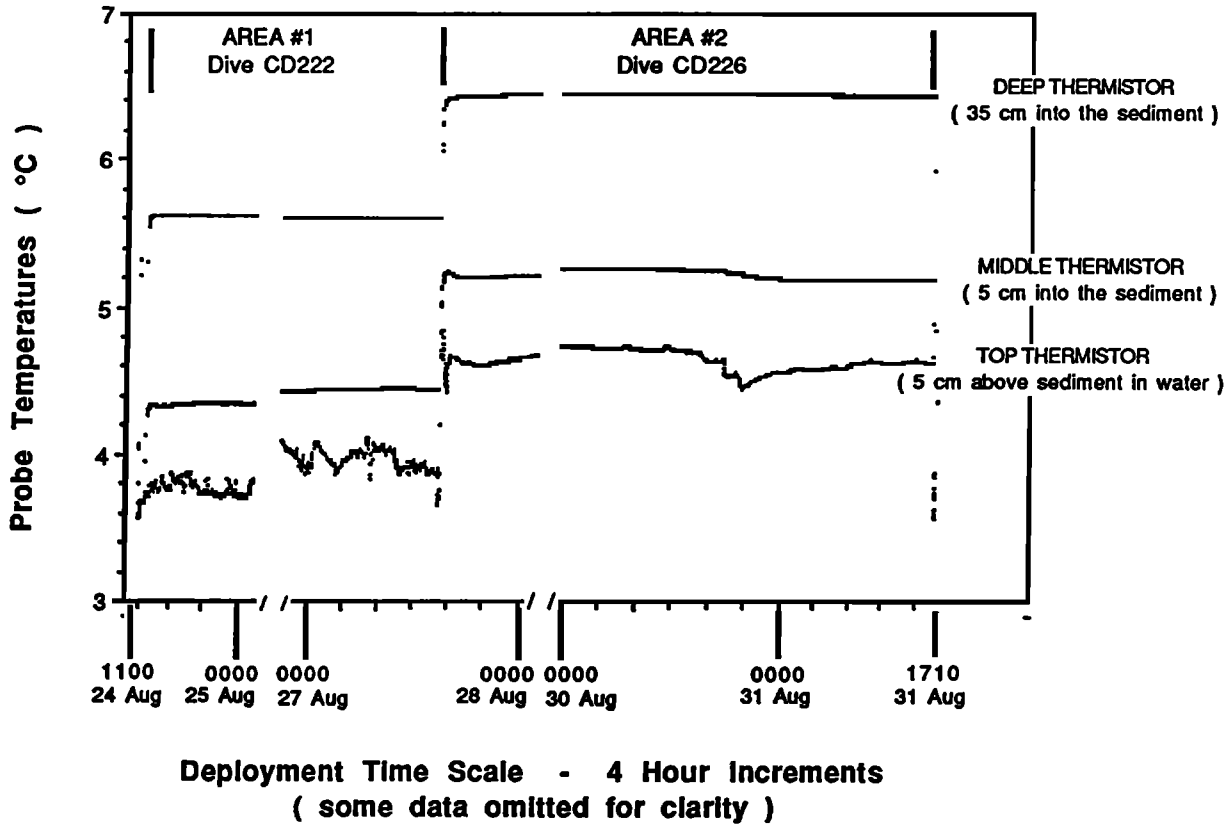

Figure 7. An abbreviated 7 day time series record of the TTT temperature probe. For clarity, we omitted data from August 25-26 and from August 28-29, 1989. Each of the thermistors in the probe measured identical values in the water column during transit. Offset in the temperature series between the two sites results from different depths that the probe penetrated.

distances of only 50 m. For example, GC 13 and BC 6 are located within 30 m of TTT 1, but the calculated velocities from the three measurements differ by three orders of magnitude (Tables 3 and 4). Another example is illustrated by BC 8, D, two gravity cores (GC 10 and 14 with pore water upwelling speeds of 3 and 8 cm yr^{-1}, respectively), and three temperature profiles (CD 216 sediment, CD 230 mat, and CD 230 pool) (Tables 1, 3, and 4). These examples are consistent with the patchy nature of observed hydrothermal features (i.e., mats, pools, and crusts).

Table 4. Average TTT Measurements for Each Day of Deployment and Calculated Velocities

Date	Area	Probe Temperature, °C -5 cm	5 cm	35 cm	Velocity, cm yr^{-1}
Aug. 24, 1989	1	3.80	4.35	5.62	-4000
Aug. 25, 1989	1	3.95	4.43	5.60	-3700
Aug. 26, 1989	1	4.03	4.43	5.6	-2900

Date	Area	Probe Temperature, °C 11 cm[a]	21 cm[a]	51 cm[a]	Velocity, cm yr^{-1}
Aug. 27, 1989	2	4.68	5.22	6.44	-1100
Aug. 28, 1989	2	4.68	5.22	6.44	-1100
Aug. 29, 1989	2	4.75	5.27	6.45	-1400
Aug. 30, 1989	2	4.63	5.19	6.44	-1000
Aug. 31, 1989	2	4.63	5.19	6.44	-1000

Negative depths are the distance above the sediment-water interface. Upwelling is negative. The adjusted depth accounts for the depth that the probe over penetrated.

[a] Adjusted depth.

Most of the cores provide evidence for pore water flow from the sediment to the deep lake, but only one core (GC 6) has chemical profiles that are concave up. These profiles are consistent with lake water that downwells through the sediment section [e.g., *Mottl*, 1989]. A downward speed of about 1 cm yr^{-1} in (5) provides the best fit to the data with an advection-diffusion model. *Redmond* [1990] suggests that the average speed of pore water downwelling across the surface area of the lake floor is about 130 cm yr^{-1}, based on mass balance calculations. Because GC 6 is located near other cores where upflow exists, we suggest that this downward moving pore water is part of a local circulation cell and does not represent a pathway for mass seepage. Local circulation cells may develop from heterogeneities in lateral pressure gradients resulting from differences in heat and pore water flow [*Wheat and McDuff*, 1994]. An alternative and less likely hypothesis is that the profiles from GC 6 are a result of a recent increase in the concentration of dissolved chemical species near the base of the core (e.g., Figure 4), presumably a product of opening and closing pathways for fluid flow.

Pore water velocities were calculated from data collected during a 7-day deployment of the TTT probe to access the degree of temporal variability in hydrothermal flow. A similar time series was recorded by *Leinen et al.* [1987] in the Mariana Mounds, a ridge-flank hydrothermal system. Both data sets

suggest that flow through the sediment is uniform for a period of at least several days. Similarly, *Schultz et al.* [1992] measured velocities of diffuse flow from a mid-ocean ridge-axis hydrothermal system in which the average velocity was uniform for periods of several days, but hourly values fluctuated with the tidal cycle. Land-based hydrothermal systems also may be affected by tidal and barometric changes [*Rinehart*, 1972]. None of these low-frequency effects are evident in the data, but some temperature fluctuations were recorded by the deepest thermistor. Pore water flow in Crater Lake must be fairly uniform for periods of at least several years, based on thriving bacterial mat assemblages that were observed during successive years. In addition, pore water chemical and thermal profiles suggest that focused flow may be maintained for tens of years. At least several tens of years are required to generate a steady state chemical profile where pore water upwells at a speed of 10 cm yr^{-1} through a theoretical 5 m thick sediment column. More time is required if upwelling speeds are slower or if the sediment column is thicker. Because sediment thickness is not known in the exact locations where cores were taken, the temporal variability of flow through the sediment is uncertain, but it must persist for decades (centuries) in areas with pore water velocities on the order of tenths of centimeters to several centimeters per year.

5.2. Fluid Flow Within the Upper Basement

We define the upper basement as the region where fluids develop their chemical signature before upwelling and diffusing through the sediment. This definition allows the upper basement to be either a permeable sedimentary layer (several meters) or igneous basement (tens to hundreds of meters) below the sampled section. Knowledge of the composition of the fluid in the upper basement provides constraints for the source or sources of thermally and chemically altered fluids that enter the lake. The composition of these fluids is estimated by extrapolating chemical profiles throughout the sediment column by fitting the data to calculations of (5) where z_{bot} is sediment thickness based on the seismic data of *Barber and Nelson* [1990] and v is the best estimate listed in Table 3. C_{bot} is then varied for the best fit to the data [e.g., *Wheat and Mottl*, 1994]. Given velocities greater than several centimeters per year, C_{bot} is simply the asymptotic concentration. Calculations of C_{bot} differ by a factor of 4 for several cores (Table 5). This difference is consistent with a reservoir model for the southern portion of Crater Lake in which lake water flows downward into basement, reacts with basement, upwells, and mixes with more lake water before entering the sediment section.

The downward seepage of lake water is probably regulated by the bulk permeability associated with fresh lava flows in the northeast section of the lake or by fracture permeability associated with the ring fracture zone in the caldera [*Bacon and Lanphere*, 1990]. In the basement reservoir the extent of chemical alteration is directly related to temperature. The composition of this fluid in basement must be uniform for a period of at least tens to hundreds of years, and it is saltier and warmer than lake water, based on pore water data and the models presented above. When this fluid upwells, it mixes with lake water below the sampled sediment section. Mixing may occur at different depths and with different ratios of the two sources, basement and lake waters. Thus different mixing ratios result in different concentrations at the base of the cores (Table 5), yet elemental ratios of water in zones of focused upflow will be maintained because lake water is much more dilute than the fluid in basement, and advective fluxes are orders of magnitude greater than reactive fluxes. This reservoir model supports a single trend in plots of one chemical species versus another in zones of focused upflow. Deviations from this single trend result from non conservative behavior in a portion of the hydrothermal system in which fluid velocities must be much slower; thus fluxes from reaction may be a significant portion of the total chemical flux for these cores. Whereas the reservoir model supports a single trend, a multiple reservoir and/or reaction model support a family of trends in plots of one chemical species versus another. The range in these trends is defined by that from the different reservoirs as indicated by data from zones of focused upflow (>100 cm yr^{-1}) and from areas with slow flow (<0.1 cm yr^{-1}).

A plot of Cl versus Na illustrates a single trend for pore water from zones of focused upflow (e.g., samples collected with the box corer, solid triangles in Figure 8) and thus supports the reservoir model. Assuming Cl is conservative, deviations from this trend result from low-temperature reactions at depth that increase the concentration of Na as the fluid ascends to the sampled section. Similar Cl/element linear relationships exist in data from cores with pore water upwelling speeds that are greater than tens of centimeters per year. Because of the paucity of data for Cl, we have plotted Li and K versus Na to illustrate these singular mixing trends in cores from zones of focused upflow (Figure 8). Note that for cores with pore water velocities less than tens of centimeters per year, several element/Na relationships may exist (e.g., Li/Na from GC 1, 2, and 3 in Figure 8). GC 1, 2, and 3 present examples of the effects of low-temperature water-sediment reactions in Crater Lake, and any pore water flow associated with these cores is a likely result of sediment compaction. These reactions add Na to the pore water, but concentrations of Li remain unchanged. With the exception of Cl, Li is the most conservative element that we measured in pore water from Crater Lake.

The reservoir model does not preclude other "reservoirs" being present under the lake. All of the data used to illustrate the presence of a single reservoir are from cores with pore water that upwells at speeds greater than about 10 cm yr^{-1} in the southern basin. Thus other reservoirs may feed hydrothermal systems in the East and North Basins. In fact, one sample with anomalously high concentrations of Na (Figure 8) was recovered by the submersible in the North Basin, but the hydrothermal system that generated this sample must have a minimal impact on heat and salt fluxes to the lake [*McManus et al.*, 1993].

Table 5. Projected Concentrations for Pore Fluids at the Base of the Sediment Column

Chemical Species	BC 6	BC 8	PD	GC 8	GC 13	Bottom Water
Na^+	0.85	2.4	2.1	4.4	3.8	0.455
Cl^-	0.57	1.2		2.1	2.0	0.274
Ca^{2+}	~0.2	~0.8	0.68	0.91	0.92	0.17
Mg^{2+}	~0.2	~1.0	0.90	0.98	0.94	0.11
K^+	0.11	0.19	0.14	0.43	0.42	0.044
Li^+	0.014	0.035	0.025	0.078	0.075	0.0066
Si	0.59	0.88	0.79	1.1	1.2	0.32

No entry denotes lack of data. Values are given in millimolars.

6. Hydrothermal Fluid and Chemical Fluxes

Hydrothermal fluid and chemical fluxes for Crater Lake are calculated using a mass balance equation of the hydrologic budget which is

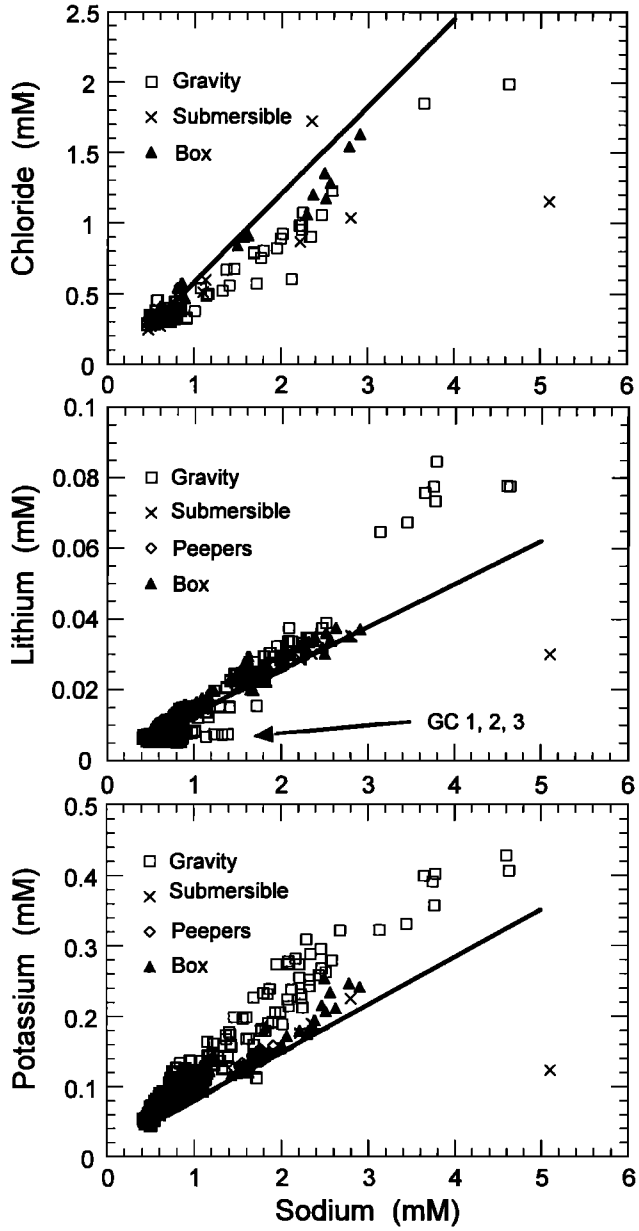

Figure 8. Concentrations of Cl, Li, and K versus Na. Lines represent mixing relationships defined by mass balance calculations. Symbols represent the different sampling techniques (open squares, gravity cores; solid triangles, box cores; open diamonds, peepers; and cross signs, submersible samples). All of the data are shown.

$$\text{precipitation} + \text{runoff} = \text{evaporation} + \text{net seepage}, \quad (10)$$

where each term represents a measured fluid flux. Net seepage of water from the lake is defined by

$$\text{net seepage} + \text{mixing} = \text{total seepage} - \text{hydrothermal} + \text{mixing}. \quad (11)$$

The mixing flux accounts for water that seeps into the upper basement, mixes with hydrothermal fluids, and upwells through the sediment column into the lake. Although the mixing terms cancel in (11), they are included because they are important in conceptualizing fluid flow through the basement. Chemical

Table 6. Fluid Flux and Chemical Parameters for Mass Balance Calculations

Water Budget	Fluid Flux 10^7 m^3 yr^{-1}	Li^+, μM	Na^+, mM	K^+, mM	Cl^-, mM
Spring runoff	2[a]	1	0.1	0.025	0.015[b]
Precipitation	11[a]	1[c]	0.013[b]	0.006[b]	0.014[b]
Evaporation	6.3[d]	0.1[e]	0.0013[e]	0.0006[e]	0.0014[e]
Net Seepage	6.7[d]	6.7	0.455	0.044	0.274
Hydrothermal	0.14	290	19	1.1	12

[a]About 85% of the fluid input is from direct precipitation [*Nathenson*, 1990] for a total input of 13.1 m^3 yr^{-1} [*Redmond*, 1990].
[b]*Simpson* [1970a].
[c]Assumes no water-rock interaction in stream runoff, thus equal to the value in stream runoff.
[d]*Redmond* [1990].
[e]Estimated to be one tenth of that in precipitation.

fluxes in the lake are defined by combining (10) and (11) and accounting for the chemical composition of each fluid flux:

$$V_{\text{hydro}}\,[C_{\text{hydro}} - C_{\text{lake}}] = C_{\text{lake}}\,V_{\text{net seepage}} + C_{\text{evap}}\,V_{\text{evap}} - C_{\text{precip}}\,V_{\text{precip}} - C_{\text{runoff}}\,V_{\text{runoff}}, \quad (12)$$

where C is concentration and V is volume flux. For Na, Cl, Li, and K we assume that (1) no terms are required for diagenetic reaction as the hydrothermal fluid upwells into the lake, (2) there are no dissolution, precipitation, adsorption, or desorption reactions in the water column, and (3) there are no dominant biogenic sources or sinks of these elements. Given the concentrations and water fluxes in Tables 6 and 7, we reduce (12) to a series of equations for each element. For example,

$$V_{\text{hydro}}\,[Na_{\text{hydro}} - Na_{\text{lake}}] = 2.7 \times 10^7 \text{ mol Na yr}^{-1}. \quad (13)$$

The dominate term in (12) is the term for net seepage, which is equal to the volumetric net flux of water to basement multiplied by the composition of lake water. The composition of lake water is known to within a few percent; however, the volumetric net seepage is probably only known to within 10-20% [*Redmond*, 1990]. Cl, Li, Na, and K fluxes from hydrothermal sources are 8.8, 2.5, 7.9, and 1.6 times, respectively, greater than the combined fluxes from precipitation and runoff. In the calculations above we assumed that diagenetic and burial fluxes

Table 7. Parameters for Mass Balance Calculations

Parameter	Value		
Volume of lake[a]	17.3 km^3		
Area of drainage basin[b]	67.8 km^2		
Area of lake[b]	53.2 km^2		
Area of lake deeper than 350 m	22.3 km^2		
Power output below 350 m, MW	15 to 31[c]	23 ± 8[d]	30 ± 5[e]

[a]*Redmond* [1990].
[b]*Phillips* [1968].
[c]The conductive power output that is not associated with the reservoir fluid is at most 3 MW [*Williams and Von Herzen*, 1983].
[d]*McManus et al.* [1993].
[e]This work.

were not significant for these elements. For example, the diagenetic flux of K to the lake based on the diffusional gradient of pore water concentrations from GC 1, 2, and 3 and the surface area of the lake is about 9% of the hydrothermal flux, whereas the depositional flux of K to the sediment-water interface is 11% of the hydrothermal flux. Similarly, the diagenetic and depositional fluxes for Na are about 4% and 3%, respectively, of the hydrothermal flux. These fluxes for Li and Cl are less than 2% of calculated hydrothermal fluxes.

We can then combine any two of these equations (e.g., (13)) to determine mixing relationships between the hydrothermal fluid in basement and lake waters (Figure 8). Provided there is primarily one source of hydrothermal fluids to the lake, the composition of the end-member hydrothermal fluid must fall along this line. Samples that best fit these linear relationships are those from box cores and peepers, which have pore water upwelling speeds that are at least an order of magnitude greater than that calculated from gravity core data. These faster flows allow less time for water-rock/sediment reactions to occur, and fluxes from these reactions are small relative to transport fluxes; thus changes in concentration are less likely to be observed [*Wheat and McDuff*, 1994]. The fit between these data and mixing lines support earlier conclusions that most of the hydrothermal input to the lake is in the southern basin [*McManus et al.*, 1993] and suggest that we located the sites of active venting that account for the observed changes in the water column. Ion-ion relationships shown in Figure 8 further illustrate the effects of low-temperature water-rock/sediment reaction on the upwelling pore water. If we assume that Cl is conservative during upwelling from basement, then these low-temperature reactions add Na, Li, and K to pore water. We expect these reactions to occur below the sampled section in an environment which is warmer than lake water, because the products of these reactions are much different than those defined by GC 1, 2 and 3 from areas with low heat and pore water flow and where flow is probably restricted to that from sediment compaction.

Equation (12) also provides a means to calculate the residence time of ions in the lake. The calculated residence time for Na, Li, K, and Cl is about 250 years. Note that these calculations are independent of the particular volume flux or concentration of the hydrothermal fluid; however, these parameters do provide some constraints on the residence time of water in the lake. For example, if the hydrothermal fluid has a concentration of 4.6 m*M* Na, the highest concentration measured in pore water samples, then the hydrothermal fluid flux is at least 5% of that from precipitation and runoff, and the residence time for water in the lake is about 130 years. If the concentration of Na were higher, then the hydrothermal water flux would be lower, but an additional flux of lake water is required to dilute this hydrothermal fluid to concentrations observed in the pore water data. The overall effect of this dilution will produce the same net result as described before. Much of the hydrothermal fluid that upwells into the lake is probably diluted to a concentration of 2.3 m*M* Na, which is consistent with results from BC 8 and D, or possibly as low as 0.85 m*M*, as observed in BC 6. This variation results in a calculated range of water residence times from 90 to 130 years and water fluxes (hydrothermal plus mixing) from 6.85×10^7 to 0.65×10^7 m^3 yr^{-1}. This net water flux from the sediments (hydrothermal plus mixing) is consistent with submersible observations of the extent of pore water flow in the southern basin. If most of the pore water flow from the sediment has a concentration of 2.3 m*M* Na and is upwelling at a speed of 200 cm yr^{-1}, as calculated from profiles of box cores and peepers, then an area of 7 km^2 is required to vent the upwelling hydrothermal fluids. This area is about 33% of the area below 350 m and is larger than expected based on observations. In contrast, pore water that flows through bacterial mats and manganese crusts has measured upwelling speeds in the range of 1000 to 14,000 cm yr^{-1}. On the basis of this range of velocities the area through which pore water must flow is about 1.5 km^2 (6.7%) to 0.10 km^2 (0.45%). A smaller area is required if flow is more focused. Considering the areal extent of mats and manganese crusts in the southern portion of the South Basin and the many high temperature measurements at less than 20 cm depth that reflect faster speeds of upwelling than the results presented herein, we can account for all of the pore water flow from the sediment, but the portion of this flow that originates as pristine hydrothermal fluid from deep within the basement is equivocal.

7. Constraints on the Composition of the Hydrothermal Fluid

The composition of the fluid in basement is constrained by the composition of the most altered pore water, elemental ratios from sites that have the fastest pore water velocities, and mass balance considerations. In this section we use these compositions and ratios in conjunction with empirical geothermometers, which are based on measured temperatures and chemical analyses of fluids from a range of land-based hydrothermal settings [e.g., *Fournier and Rowe*, 1966; *Fouillac and Michard*, 1981; *Fournier*, 1981, 1990; *Giggenbach*, 1988; *Kharaka and Mariner*, 1989], to place limits on the maximum extent of chemical alteration of the hydrothermal fluid and to estimate the temperature at depth in basement. Determining thermodynamic boundaries for mineral phases is not in the purview of this paper, which focuses solely on the subsurface flow regime as constrained by pore water chemical and thermal data.

Two geothermometers use concentrations of Li and Na to predict fluid temperature [*Fouillac and Michard*, 1981]:

$$\text{Log (Na/Li)} = -0.38 + 1000 / [T(^\circ\text{C}) + 273.15], \quad (14)$$

$$\text{Log (Li)} = 1.44 - 2258 / [T(^\circ\text{C}) + 273.15], \quad (15)$$

where concentrations are in molar units. Another geothermometer is based on Na/K. We used *Truesdell*'s [1976] equation:

$$\text{Log (Na/K)} = -0.8573 + 855.6 / [T(^\circ\text{C}) + 273.15], \quad (16)$$

where concentrations are in units of milligrams per kilogram, because it provides the best fit to data below 250°C, yet it provides a poor measure if temperatures are below 150°C. We chose these three geothermometers because (1) our samples are from surface expressions of venting that are susceptible to chemical alteration while upwelling into the lake, in contrast to samples from boreholes that provide a means for collecting pristine fluids from basement and are the basis for geothermometers and (2) they include the least reactive elements in pore waters from box cores and peepers collected in the Crater Lake system from which a geotemperature can be calculated. Measured concentrations of Li substituted into (15) result in calculated temperatures that range from 65° to 135°C. These temperatures are minimums because dilution of the hydrothermal fluid with lake water lowers the concentration and thus the calculated temperature. By substituting Li/Na and K/Na ratios defined by mass balance calculations (equation (13)) into (14) and (16), calculated temperatures are 166°C and 197°C, respectively. Low-temperature water-rock/sediment

reactions in Crater Lake result in lower Li/Na and higher K/Na; thus 160°C is likely to be a lower bound, and 200°C is likely to be an upper bound. If we use the average temperature of 180°C in (14) through (16), then the end-member hydrothermal fluid has a composition of 19 m*M* Na. Given a 19 m*M* Na hydrothermal fluid and the mass balance equation (13), the composition of the hydrothermal fluid is 0.24 m*M* Li, 1.2 m*M* K, and 12 m*M* Cl. Mixing lines between this fluid and lake water fit the pore water data from box core and peeper samples (Figure 8). As noted above, these samples represent the most pristine fluids from basement.

Other geothermometers such as Si [*Fournier and Rowe*, 1966, 1977], Na-K-Ca-Mg [*Fournier and Potter*, 1979], K-Mg [*Giggenbach*, 1988], and Na-K-Mg [*Fournier*, 1990] have been developed but are inappropriate for use with samples from Crater Lake, because the rate of reaction of Si, Ca, and Mg within sediment and basement is fast enough and too complex to reduce the data to a single trend that can then be used in calculations for the temperature at depth.

Given a temperature of 180°C in the reservoir and the geothermometers listed in (14)-(16), we calculated a basement reservoir concentration for Li, Na, and K. By substituting this concentration into appropriate equations that are similar to (13), we calculate the volumetric hydrothermal fluid influx to the lake. This fluid flux coupled with a temperature of 180°C results in a total power input to the lake of 30 ± 5 MW. This calculation is based solely on geothermometers and general hydrologic mass balance data and is consistent with (1) elemental ratios of pore water concentrations from zones of focused upflow; (2) *Williams and Von Herzen*'s [1983] estimate of 15 to 31 MW, based on 62 measurements of sediment heat flow and temperature profiles in the water column; and (3) *McManus et al.*'s [1993] estimate of 23±8 MW, based on the water column thermal inventory. The agreement between these three estimates is significant, because all three estimates are based on different data sets and techniques. Further, this agreement provides credibility to our estimate of the temperature and composition of the hydrothermal fluid. In addition, our calculated temperature, which is about 10 times the highest measured temperature, is in the range of that predicted by *Williams and Von Herzen* [1983], who estimated a temperature of 100° to 200°C at a depth of 1.5 to 2 km; dilution with cold lake water and loss of heat via conduction lowers the temperature to measured levels. Alternatively, if the end-member fluid is represented by the most altered pore water (4.6 m*M* Na), then (13) allows one to calculate the volumetric hydrothermal flux, and the temperature of this fluid must be 39°C to generate 30 MW or 31°C to generate the 23 MW reported by *McManus et al.* [1993]. These temperatures, which must be considered lower limits, are much lower than temperatures estimated from the data and the geothermometers listed above (equations (14)-(16)). Further, concentrations of Li in pore water and the positive Eu anomaly observed in spring samples suggest a much higher temperature [*Collier et al.*, 1991]. Taking these caveats into consideration, we reiterate that the three geothermometers used above coupled with mass balance considerations are in and of themselves independent of the pore water, heat flow, and water column data and that a temperature of about 180°C provides the best fit to the data and constraints.

8. Conclusions

On the basis of systematic variations in pore water chemical and thermal properties, we have presented evidence that supports the input of hydrothermal fluid into Crater Lake, Oregon. Pore water issues from the lake floor at speeds of tenths of a centimeter per year to tens of thousands of centimeters per year and are derived from mixing deep lake water with thermally and chemically altered fluids from basement. We have estimated a hydrothermal end-member temperature and composition based on geothermometers and mass balance calculations. When these compositions are substituted into flux equations (e.g., (13)), a volumetric hydrothermal flux is calculated.

This study illustrates the power of pore water chemical data and thermal profiles in sediment to constrain the pattern of fluid circulation in a hydrothermal setting. Similar studies have been conducted in hydrothermal systems on the flanks of the mid-ocean ridge axes [e.g., *Wheat and Mottl*, 1994; *Wheat and McDuff*, 1995], and the same techniques employed herein are applicable to groundwater flow into fresh and estuarine water. One of the most important parameters that is elucidated by these techniques is an estimate for the chemical composition of the fluid in basement. This composition then constrains the path for fluid flow, the extent of reaction in basement, and mass, thermal, and chemical fluxes from fluid circulation.

Acknowledgments. Many individuals contributed their time and effort during the field and laboratory portions of this work. The authors are particularly appreciative of the generous help provided by M. Buktenica, J. Milestone, and the rest of the lake crew at Crater Lake National Park. G. Whipple and C. Meredith provided analytical assistance. C. G. W. is indebted to R. McDuff for financial support during the field portion of this program. We greatly appreciate the thoughtful reviews from D. Issler, I. Hutcheon, and an anonymous reviewer. This research was funded by the U.S. National Park Service under cooperative agreement CA 9000-3-0003, CPSU, College of Forestry, Oregon State University. IMS, University of Alaska Fairbanks contribution 2488.

References

Bacon, C. R., Eruptive history of Mount Mazama and Crater Lake Caldera, Cascade Range, U.S.A., *J. Volcanol. Geotherm. Res.*, *18*, 57-115, 1983.

Bacon, C. R., and M. A. Lanphere, The geologic setting of Crater Lake, Oregon, in *Crater Lake: An Ecosystem Study*, edited by E. T. Drake, et al., pp. 19-27, Pac. Div. Am. Assoc. for the Adv. of Sci., San Francisco, 1990.

Barber, J. H., and C. H. Nelson, Sedimentary history of Crater Lake Caldera, Oregon, in *Crater Lake: An Ecosystem Study*, edited by E. T. Drake, et al., pp. 29-39, Pac. Div. Am. Assoc. for the Adv. of Sci., San Francisco, 1990.

Bender, M., W. Martin, J. Hess, F. Sayles, and L. Ball, A whole core squeezer for interfacial pore water sampling, *Limnol. Oceanogr.*, *32*, 1214-1225, 1987.

Berner, R. A., *Early Diagenesis*, 241 pp., Princeton Univ. Press, Princeton, N. J., 1980.

Boudreau, B. P., Asymptotic forms and solutions of the model for silica-opal diagenesis in bioturbated sediments, *J. Geophys. Res.*, *95*, 7367-7379, 1990.

Collier, R., J. Dymond, J. McManus, R. Conrad, C. Meredith, and G. Wheat, Mass balances and geochemical fluxes derived from hydrothermal activity in Crater Lake, OR (abstract), *Eos Trans. AGU*, *71*, 1674, 1990a.

Collier, R., J. Dymond, J. McManus, and J. Lupton, Chemical and physical properties of the water column at Crater Lake, Oregon, in *Crater Lake: An Ecosystem Study*, edited by E. T.

Drake, et al., pp. 69-79, Pac. Div. Am. Assoc. for the Adv. of Sci., San Francisco, 1990b.

Collier, R., J. Dymond, and J. McManus, Studies of Hydrothermal Processes in Crater Lake, OR, Rep. [90-7], pp. 201 Pac. NW Reg., Nation. Park Serv., Seattle, Wash, 1991.

de Lange, G. J., R. E. Cranston, D. H. Mydes, and D. Boust, Extraction of pore water from marine sediments: A review of possible artifacts with pertinent examples from the North Atlantic, *Mar. Geol.*, *109*, 53-76, 1992.

Dymond, J., and R. W. Collier, The chemistry of Crater Lake sediments: Definition of sources and implications for hydrothermal activity, in *Crater Lake: An Ecosystem Study*, edited by E. T. Drake, et al., pp. 41-60, Pac. Div. Am. Assoc. for the Adv. of Sci., San Francisco, 1990.

Dymond, J., R. W. Collier, and M. E. Watwood, Bacterial mats from Crater Lake, Oregon and their relationship to possible deep-lake hydrothermal venting, *Nature, 342*, 673-675, 1989.

Fouillac, C., and G. Michard, Sodium/lithium ratio in water applied to geothermometry of geothermal reservoirs, *Geothermics, 10*, 55-70, 1981.

Fournier, R. O., Application of water geochemistry to geothermal exploration and reservoir engineering, in *Geothermal Systems: Principles and Case Histories*, edited by L. Rybach and J. P. Muffler, pp. 109-143, John Wiley, New York, 1981.

Fournier, R. O., The interpretation of Na-K-Mg relations in geothermal waters, *Trans. Geotherm. Resour. Counc., Part II, 14*, 1421-1425, 1990.

Fournier, R. O., and R. W. Potter, Magnesium correction to the Na-K-Ca chemical geothermometer, *Geochim. Cosmochim. Acta, 43*, 1543-1550, 1979.

Fournier, R. O., and J. J. Rowe, Estimation of underground temperatures from the silica content of water from hot springs and wet-steam wells, *Am. J. Sci., 264*, 685-697, 1966.

Fournier, R. O., and J. J. Rowe, The solubility of amorphous silica in water at high temperatures and high pressures, *Am. Mineral., 62*, 1052-1056, 1977.

Giggenbach, W. F., Geothermal solute equilibria: Derivation of Na-K-Mg-Ca geoindicators, *Geochim. Cosmochim. Acta, 52*, 2749-2765, 1988.

Kharaka, Y. K., and R. H. Mariner, Chemical geothermometers and their application to formation waters from sedimentary basins, in *Thermal History of Sedimentary Basins: Methods and Case Histories*, edited by N. D. Naeser and T. H. McCulloh, pp. 99-117, Springer-Verlag, New York, 1989.

Leinen, M. L., R. E. McDuff, K. Becker, and P. Schultheiss, Off-axis hydrothermal activity in the Mariana Mounds Field (abstract), *Eos Trans. AGU, 68*, 1531, 1987.

Li, Y.-H., and S. Gregory, Diffusion of ions in seawater and in deep-sea sediments, *Geochim. Cosmochim. Acta, 38*, 703-714, 1974.

McDuff, R. E., and R. A. Ellis, Determining diffusion coefficients in marine sediments: A laboratory study of the validity of resistivity techniques, *Am. J. Sci., 279*, 666-675, 1979.

McManus, J., R. Collier, C.-T. A. Chen, and J. Dymond, Physical properties of Crater Lake, OR: The determination of a conductivity- and temperature-dependent expression for salinity, *Limnol. Oceanogr., 37*, 41-53, 1992.

McManus, J., R. Collier, and J. Dymond, Mixing processes in Crater Lake, Oregon, *J. Geophys. Res., 98*, 18295-18307, 1993.

McManus, J., R. Collier, J. Dymond, C. G. Wheat, and G. L. Larson, Spatial and temporal distribution of dissolved oxygen in Crater Lake, Oregon, *Limnol. Oceanogr., 41*, 722-731, 1996.

Mottl, M. J., Hydrothermal convection, reaction, and diffusion in sediments on the Costa Rica Rift Flank: Pore-water evidence from ODP Sites 677 and 678, *Proc. Ocean Drill. Program Sci. Results, 111*, 195-213, 1989.

Nathenson, M., Chemical balance for the major elements in water in Crater Lake, Oregon, in *Crater Lake: An Ecosystem Study*, edited by E. T. Drake, et al., pp. 103-114, Pac. Div. Am. Assoc. for the Adv. of Sci., San Francisco, 1990.

Parsons, T. R., Y. Maita, and C. M. Lalli, *A Manual of Chemical and Biological Methods for Seawater Analysis*, 173 pp., Pergamon, Tarrytown, New York, 1984.

Phillips, K. N., Hydrology of Crater, East, and Davis Lakes, Oregon, *U.S. Geol. Surv. Water Supply Pap., 1859-E*, 60 pp., 1968.

Redmond, K. T., Crater Lake climate and lake level variability, in *Crater Lake: An Ecosystem Study*, edited by E. T. Drake, et al., pp. 127-141, Pac. Div. Am. Assoc. for the Adv. of Sci., San Francisco, 1990.

Rinehart, J. S., Fluctuations in geyser activity caused by variations in Earth tidal forces, barometric pressure, and tectonic stresses, *J. Geophys. Res., 77*, 342-350, 1972.

Schultz, A., J. R. Delaney, and R. E. McDuff, On the partitioning of heat flux between diffusive and point source seafloor venting, *J. Geophys. Res., 97*, 12299-12314, 1992.

Simpson, H. J., Closed basin lakes as a tool in geochemistry, 325 pp., Ph.D. dissertation, Columbia Univ., New York 1970a.

Simpson, H. J., Tritium in Crater Lake, Oregon, *J. Geophys. Res., 75*, 5195-5207, 1970b.

Soutar, A., S. Johnson, K. Fischer, and J. Dymond, Sampling the sediment-water interface: Evidence for an organic-rich surface layer (abstract), *Eos Trans. AGU, 62*, 905, 1981.

Truesdell, A. H., Summary of section III - geochemical techniques in exploration, in *Second United Nations Symposium on the Development and Use of Geothermal Resources, May, 1975*, 1, 1iii-1xiii, San Francisco, 1976.

Van Denburgh, A. S., Chemistry of the lakes, in *Hydrology of Crater, East, and Davis Lakes, Oregon*, edited by K. N. Phillips,*U.S. Geol. Surv. Water Supply Pap., 1859-E*, 41-44, 1968.

Wheat, C. G., and R. E. McDuff, Hydrothermal flow through the Mariana Mounds: Dissolution of amorphous silica and degradation of organic matter on a mid-ocean ridge flank, *Geochim. Cosmochim. Acta, 58*, 2461-2475, 1994.

Wheat, C. G., and R. E. McDuff, Mapping the fluid flow of the Mariana Mounds ridge flank hydrothermal system: Pore water chemical tracers, *J. Geophys. Res., 100*, 8115-8131, 1995.

Wheat, C. G., and M. J. Mottl, Hydrothermal circulation, Juan de Fuca Ridge Eastern Flank: Factors controlling basement water composition, *J. Geophys. Res., 99*, 3067-3080, 1994.

Williams, D. L., and R. P. Von Herzen, On the terrestrial heat flow and physical limnology of Crater Lake, Oregon, *J. Geophys Res., 88*, 1094-1104, 1983.

R. Collier, J. Dymond, and J. McManus, College of Oceanic and Atmospheric Sciences, Oregon State University, Corvallis, OR 97331-5503. (e-mail: collier @oce.orst.edu; dymond@oce.orst.edu; mcmanus@oce.orst.edu).

C. G. Wheat, West Coast and Polar Regions Undersea Research Center, P.O. Box 475, Moss Landing, CA 95039. (e-mail: wheat@mbari.org).

M. Whiticar, Centre for Earth and Ocean Research, University of Victoria, P.O. Box 1700, Victoria, British Columbia, Canada V8W 2Y2 (e-mail: whiticar@uvphys.phys.uvic.ca).

(Received November 11, 1996; revised November 2, 1997; accepted November 17, 1997.)